Appendix A

Perturbative View of BPM data Decomposition

Taylor expanding 'b' over all physical variables:

$$\begin{aligned} b - \langle b \rangle &= \sum_{v} \left.\frac{\partial b}{\partial v}\right|_{v=\overline{v}} (\Delta v - \langle \Delta v \rangle) \\ &+ \frac{1}{2} \sum_{v_1, v_2} \left.\frac{\partial^2 b}{\partial v_2 \partial v_1}\right|_{v=\overline{v}} (\Delta v_1 \Delta v_2 - \langle \Delta v_1 \Delta v_2 \rangle) \\ &+ \ldots \end{aligned}$$

where b is a function of $\overline{x}, \overline{x}', \overline{\delta}, \overline{\sigma}_z$ and other physical physical variables.

Treating 1^{st} and 2^{nd} order terms the same (higher-order negligible):

$$b - \langle b \rangle = \sum_{(q)} q f_q \tag{A.1}$$

where

$$q = \frac{\Delta v - \langle \Delta v \rangle}{std(\Delta v)} \tag{A.2}$$

$$= \frac{\Delta v_1 \Delta v_2 - \langle \Delta v_1 \Delta v_2 \rangle}{std(\Delta v_1 \Delta v_2)}, \tag{A.3}$$

and

$$f_q = \left.\frac{\partial b}{\partial v}\right|_{v} std(\Delta v) \tag{A.4}$$

$$= \left.\frac{\partial^2 b}{\partial v_2 \partial v_1}\right|_{v_1 v_2} std(\Delta v_1 \Delta v_2) \tag{A.5}$$

Eq. A.1 in matrix notation is simply

$$B = W V^T \tag{A.6}$$

Appendix B

Geometric view of coupled SVD modes

Since, the SVD modes are approximately linear combinations of the spatial eigenmodes, it is interesting to view the evolution spatial vectors for each axes in terms of a parametric plots as shown Fig. B.1 In the absence of coupling,

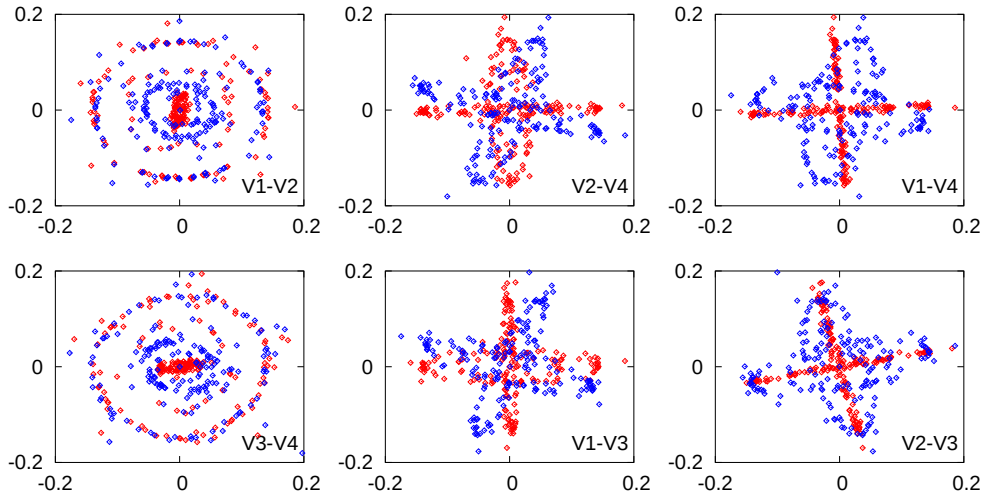

Figure B.1: Parametric plots of SVD modes of BPM data from each plane (x-red, y-blue). Data taken using ac dipoles during Run-2004.

parametric plots should simply exhibit orthogonal lines lying on the coordinate axes. The rotation with respect to the coordinate axes and the finite width to the ellipses point to non-zero coupling present in the lattice.

A simple inference from these plots can be made that there are approximately two angles of rotation (ϕ_1 and ϕ_2) by which the spatial vectors are rotated w.r.t to each other. One can construct a simple orthogonal rotation

matrix $O_{4\times4}$ given by

$$\begin{bmatrix} \cos\phi_1 & 0 & -\sin\phi_1 & 0 \\ 0 & \cos\phi_2 & 0 & -\sin\phi_2 \\ \sin\phi_1 & 0 & \cos\phi_1 & 0 \\ 0 & \sin\phi_2 & 0 & \cos\phi_2 \end{bmatrix} \tag{B.1}$$

which will rotate the SVD modes into the physical eigenmodes Although, this approach maybe more intuitive, one has to rely on fitting techniques to accurately determine these angles. The harmonic projection is in the frequency domain is far simpler and probably yield a numerically more accurate O matrix. Nevertheless, the outcome of this parametric plots are interesting.

Appendix C

Coupling Matrix

C.1 Propagation of the $\overline{\mathbf{C}}$ matrix

In a coupler free region $\overline{\mathbf{C}}$ matrix is simply propagated by an arbitrary phase advance in both modes which is given by [42]

$$\overline{\mathbf{C}}_{\mathbf{2}} = \mathbf{R}_x(\phi_x)\overline{\mathbf{C}}_{\mathbf{1}}\mathbf{R}_y^{-1}(\phi_y) \tag{C.1}$$

where $\mathbf{R_{x,y}} = \begin{pmatrix} \cos\phi_{x,y} & \sin\phi_{x,y} \\ -\sin\phi_{x,y} & \cos\phi_{x,y} \end{pmatrix}$.

If coupling is small and couplers modeled as thin skew quadrupoles, the $\overline{\mathbf{C}}$ is propagated to first order given by [50]

$$\overline{\mathbf{C}}_{\mathbf{2}} = \overline{\mathbf{C}}_{\mathbf{1}} - \overline{\mathbf{k}} \tag{C.2}$$

where

$$\overline{\mathbf{k}} = \begin{pmatrix} 0 & 0 \\ \overline{k} & 0 \end{pmatrix} \tag{C.3}$$

with $\overline{k} = \sqrt{\beta_a^{skew}\beta_b^{skew}}k$ and k is the strength of the coupler. Here γ is assumed to be 1.

C.2 Normalized momenta

The normalized momenta $\hat{p}_{x,y}$ are given by the normalized positions at a location $\pi/2$ apart. This location does not have to correspond to any physical location. To compute $\hat{p}_x$ the $\overline{\mathbf{C}}$ matrix is propagated by $\pi/2$ in the horizontal mode and an arbitrary ϕ_y in the vertical mode

$$\begin{aligned} \overline{\mathbf{C}}' &= \mathbf{R}_x(\pi/2)\mathbf{C}\mathbf{R}_y^{-1}(\phi_y) \\ &= \begin{pmatrix} \overline{C}_{21}c\phi_y + \overline{C}_{22}s\phi_y & -\overline{C}_{21}s\phi_y + \overline{C}_{22}c\phi_y \\ -\overline{C}_{11}c\phi_y - \overline{C}_{12}s\phi_y & \overline{C}_{11}s\phi_y - \overline{C}_{12}c\phi_y \end{pmatrix} . \end{aligned} \tag{C.4}$$

where $c\phi = \cos(\phi)$ and $s\phi = \sin(\phi)$. Therefore, $\hat{p}_x$ is obtained by using $\hat{x}$ and $\overline{\mathbf{C}}'$ as the $\overline{\mathbf{C}}$ matrix at the new location,

$$\begin{aligned}\hat{p}_x &= \gamma A_x \cos(\psi_x + \pi/2) + \\ &\quad A_y\Big((\overline{C}_{21}\cos\phi_y + \overline{C}_{22}\sin\phi_y)\cos(\psi_y+\phi_y) - \\ &\quad (-\overline{C}_{21}\sin\phi_y + \overline{C}_{22}\cos\phi_y)\sin(\psi_y+\phi_y)\Big) \\ &= -\gamma A_x \sin\psi_x + \\ &\quad A_y\Big(\overline{C}_{21}\cos\psi_y - \overline{C}_{22}\sin\psi_y\Big)\ . \end{aligned} \tag{C.5}$$

Note that the arbitrary ϕ_y has canceled out and $\hat{p}_x$ only depends on parameters evaluated at the initial physical location. Similarly for $\hat{p}_y$,

$$\begin{aligned}\hat{p}_y &= -\gamma A_y \sin\psi_y + \\ &\quad A_x\Big(\overline{C}_{21}\cos\psi_x + \overline{C}_{11}\sin\psi_x\Big)\ . \end{aligned} \tag{C.6}$$

C.3 $\overline{C}_{21}$ in coupler free region

Using Eq. (C.1), $\overline{\mathbf{C}}$ matrix elements at two locations are related in terms of the phase advance alone which is expressed as,

$$\begin{pmatrix} C_{11}^{(2)} \\ C_{12}^{(2)} \\ C_{21}^{(2)} \\ C_{22}^{(2)} \end{pmatrix} = \begin{pmatrix} c\phi_x c\phi_y & c\phi_x s\phi_y & s\phi_x c\phi_y & s\phi_x s\phi_y \\ -c\phi_x s\phi_y & c\phi_x c\phi_y & -s\phi_x s\phi_y & s\phi_x c\phi_y \\ -s\phi_x c\phi_y & -s\phi_x s\phi_y & c\phi_x c\phi_y & c\phi_x s\phi_y \\ s\phi_x s\phi_y & -c\phi_x c\phi_y & -c\phi_x s\phi_y & c\phi_x c\phi_y \end{pmatrix} \times \begin{pmatrix} C_{11}^{(1)} \\ C_{12}^{(1)} \\ C_{21}^{(1)} \\ C_{22}^{(1)} \end{pmatrix}\ , \tag{C.7}$$

where $c\phi = \cos(\phi)$ and $s\phi = \sin(\phi)$. Given two BPM locations at which turn-by-turn data is recorded, $\overline{C}_{12}/\gamma$, $\overline{C}_{11}/\gamma$, and $\overline{C}_{22}/\gamma$ are calculated as illustrated in section 4.3.1. The phase advances between the two locations can also be determined using SVD techniques from the same turn-by-turn data [53]. Rearranging the second row of Eq. (C.7), $\overline{C}_{21}/\gamma$ is exactly calculated

in a coupler free region which is given by

$$\begin{aligned}\overline{C}_{21}^{(1)} &= \Big(-\overline{C}_{11}^{(1)} \cos\phi_a \sin\phi_b + \overline{C}_{12}^{(1)} \cos\phi_a \sin\phi_b \\ &\quad + \overline{C}_{22}^{(1)} \sin\phi_a \cos\phi_b - \overline{C}_{12}^{(2)} \Big) / (\sin\phi_a \sin\phi_b)\end{aligned} \tag{C.8}$$

C.4 Skew quadrupole strength from two BPMs

Using Eq. (C.1) and (C.2), $\overline{\mathbf{C}}$ matrix is propagated between two observation points with one skew quadrupole between them given by

$$\begin{aligned}\overline{\mathbf{C}}_{\mathbf{2}} &= \mathbf{R}_x(\phi_x^{skew+l}) \\ &\quad \times \Big[\mathbf{R}_x(\phi_x^{skew-l}) \overline{\mathbf{C}}_{\mathbf{1}} \mathbf{R}_y^{-1}(\phi_y^{skew-l}) - \overline{\mathbf{k}} \Big] \\ &\quad \times \mathbf{R}_y^{-1}(\phi_y^{skew+l})\end{aligned} \tag{C.9}$$

where $\phi_{x,y}^{skew\mp l}$ are the phase advances between the skew quadrupole and locations 1 and and 2 respectively. Determinants are distributive ($|\mathbf{AB}| = |\mathbf{A}| \times |\mathbf{B}|$), therefore

$$|\overline{\mathbf{C}}_{\mathbf{2}}| = |\mathbf{R}_x(\phi_x^{skew-l}) \overline{\mathbf{C}}_{\mathbf{1}} \mathbf{R}_y^{-1}(\phi_y^{skew-l}) - \overline{\mathbf{k}}| \tag{C.10}$$

since, $|\mathbf{R}_x(\phi_{x,y})| = 1$. Using Eq. (C.7) and (C.10) $\bar{k}$ is expressed as

$$\bar{k} = -\frac{|C^{(2)}| - |C^{(1)}|}{C_{12}^{skew}} \ , \tag{C.11}$$

which is equivalent to Eq.(4.42) derived from RDT's given that $\gamma = 1$.

Appendix D

Five-Cell SRF Cavity

D.1 Bead Pull for Fundamental Mode

In this technique, a small bead (radius $<< \lambda$) is introduced in the cavity to perturb the field which changes the resonant frequency proportional to the fields [120]. The frequency of a mode is commonly measured from scattering parameter S_{21} with a network analyzer. An equivalent and sometimes more sensitive measurement would be the phase shift of S_{21} at the unperturbed resonant frequency. The S_{21} is given by

$$S_{21} = \frac{2\sqrt{\beta_1\beta_2}}{(1+\beta_1+\beta_2) + iQ_0\left(\frac{\omega}{\omega_0} - \frac{\omega_0}{\omega}\right)} \tag{D.1}$$

where β_1 and β_2 are the coupling coefficients of input and output probes. If coupling is weak ($\beta_1, \beta_2 << 1$) and $\Delta\omega/\omega << 1$. then the change in frequency can be expressed as

$$\frac{\delta\omega}{\omega_0} \approx -\frac{1}{2Q_L} tan(\phi) \tag{D.2}$$

For spherical bead:

$$\frac{\delta\omega}{\omega_0} \quad = \quad \begin{cases} -\frac{\pi r^3}{U}(\epsilon_0 \frac{\epsilon_r+2}{\epsilon_r-1} E_0^2) & : \quad dielectric \\ -\frac{\pi r^3}{U}(\epsilon_0 E_0^2 - \frac{\mu_0}{2} H^2) & : \quad metal \end{cases} \tag{D.3}$$

By mapping the longitudinal electric field and using Eq. E.1, the shunt impedance can be calculated using

$$\frac{R}{Q}_{sphere} = -\frac{1}{2\pi\omega_0 r^3 \epsilon_0} [\int \sqrt{\frac{\delta\omega}{\omega_0}} \cos(kz) dz]^2 \tag{D.4}$$

D.2 BNL II - Alternate Design

A comparison of the broadband impedance spectrum for both longitudinal and transverse modes calculated using ABCI are shown in Fig. D.1 for BNL I, I-A and II designs as listed in Table 8.2. BNL I and I-A are essentially similar in geometry accept for subtle change in the end cell. Therefore, the impedance spectrum correspondingly looks similar. The spectrum for BNL

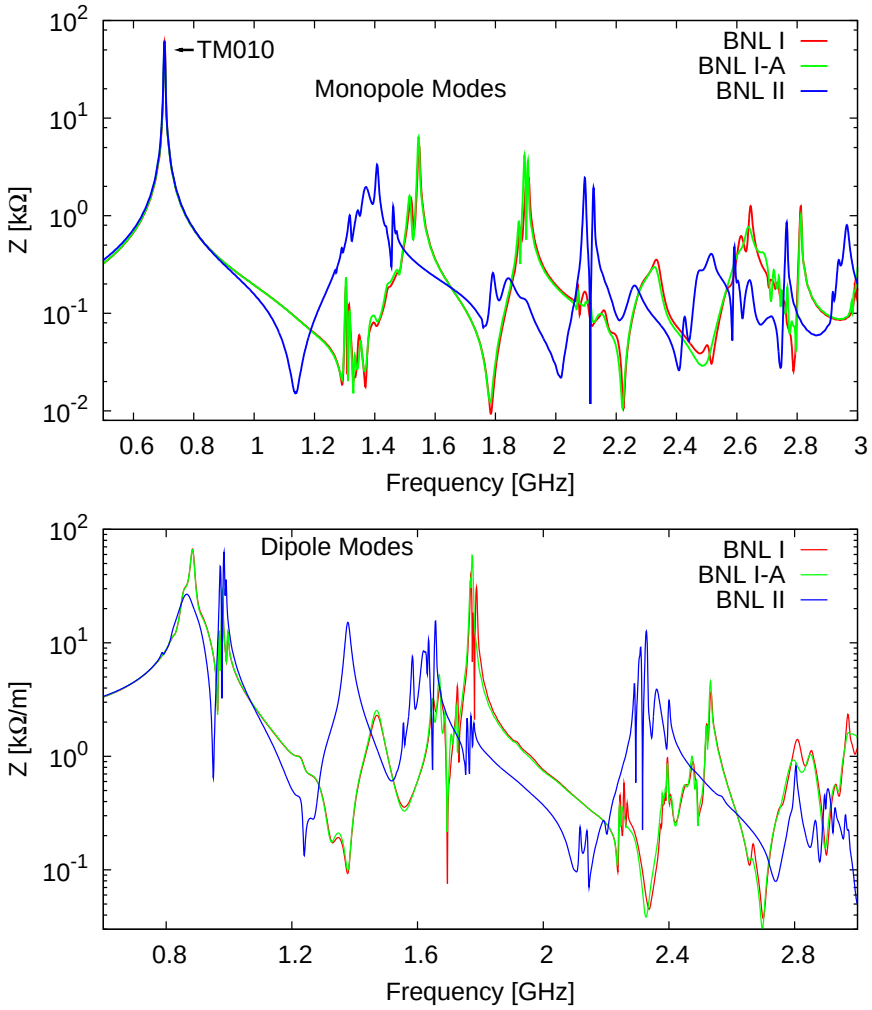

Figure D.1: Broadband impedance for monopole and dipole modes computed by ABCI for BNL I, I-A, and II designs.

II looks quite different for both monopole and dipole modes. For monopole

modes, the impedance peaks seems to have shifted to a lower frequency but the amplitude is similar to that of BNL I. In the case of dipole modes, the spectrum for BNL II shows smaller impedance values for the $5^{th} - 6^{th}$ passbands, but the larger for $2^{nd} - 3^{rd}$ and $8^{th} - 10^{th}$ passbands.

D.3 Bellow Shielding

Bellows are added on the beam pipe section of the five-cell cavity to allow longitudinal and transverse motion during cool down, warm up, alignment and transportation. The bellows are made of copper plated stainless steel. The primary power losses in these bellows can occur from surface currents of the fundamental mode and single bunch losses induced by the passage of beam. The beam pipe transition and the cold to warm transition section is designed to allow no more than 10 W of fundamental power being dissipated in bellow section. A counter flow of He gas on the beam pipe acts as a heat exchanger which is extracted out at 300 K.

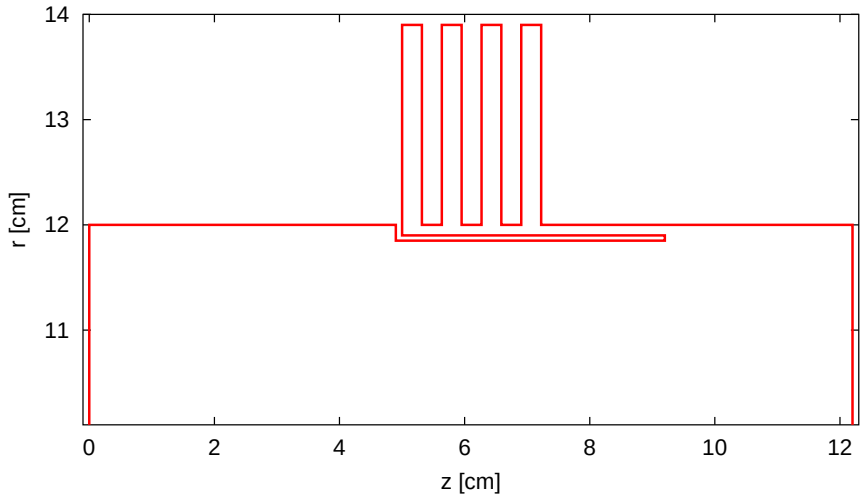

Figure D.2: A simple shielding mechanism for the bellows in the 5 K helium region.

Two sets of bellows, one right after the Niobium-Stainless Steel transition (5 K) with and one before the transition to room temperature (300 K). Several shielding mechanisms including capacitive finger were considered if shielding was necessary to reduce further losses. Fig. D.2 shows a simple shielding mechanism and a comparison of integrated loss factor is shown in Fig. D.3.

Note that the rectangular bellows were taken as an approximation to the elliptical bellows used in the cryomodule. It is clear that shielding suppress the overall power loss by an order of magnitude, but the unshielded bellows only contribute $k_{||} = 3.8 \times 10^{-2}$ which amounts to ≈ 10 W of power which is quite small. To further reduce He losses, the bellow section in the 5 K region maybe reduced to two convolutions.

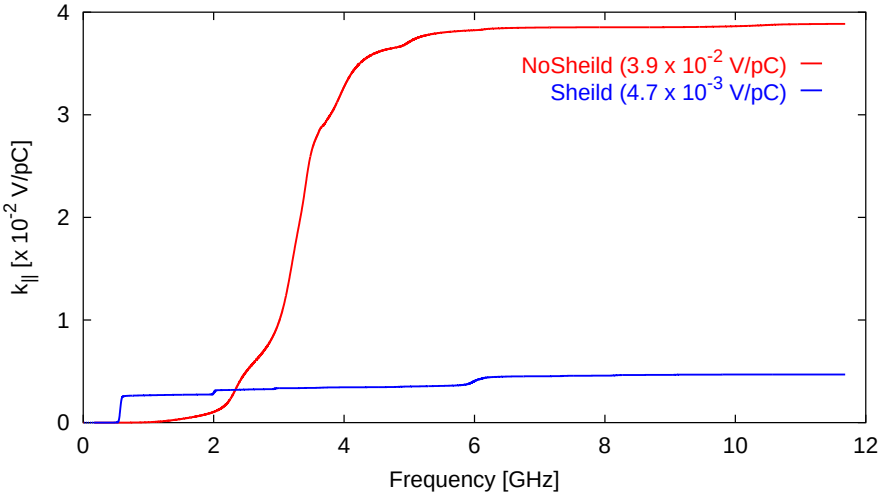

Figure D.3: A simple shielding mechanism for the bellows in the 5 K helium region.

Appendix E

$\frac{1}{2}$-Cell SRF Gun

E.1 Loss Factor Correction for $\beta < 1$

The loss factors in section II B has been calculated for ultra relativistic bunches through the gun. Since the gun will accelerate relatively long bunches (1 cm) and has a fairly large beam pipe aperture (5 cm), the loss factors were assumed to be an upper limit. Modal loss factors for $\beta < 1$ and $\beta = 1$ were calculated using the analytical expression derived in Ref. [145] given by

$$k(\beta, \sigma) = \sum_{n=1}^{n} \frac{\omega_n R_s(\beta)}{4Q_n} \; e^{-(\frac{\omega_n \sigma}{\beta c})^2}. \tag{E.1}$$

where ω_n and R_s/Q_n are the frequency and the shunt impedance (accelerator definition) of the n^{th} mode respectively and σ is the bunch length. Fig. E.1 shows a comparison between analytical expression ($\beta < 1$, $\beta = 1$) and numerical calculation ($\beta = 1$) using ABCI [124, 125] for modes below the cut-off frequencies of the beam pipe for a bunch length of 1 cm. The loss factors are clearly over estimated for $\beta = 1$ compared to $\beta < 1$. However, we use the total loss factor calculated by ABCI as the upper limit since it is difficult to analytically estimate the loss factor for modes above cut-off.

E.2 Amplitude and Phase Modulation

The effects of random fluctuations have been extensively studied in signal processing theory. Several interesting models for random processes and its effects can be found in Ref. [146]. We will assume that the beam harmonics can be represented by an infinite train of pulses with a pulse shape $p(t)$. Any modulation of the laser amplitude and/or phase will manifest itself as a

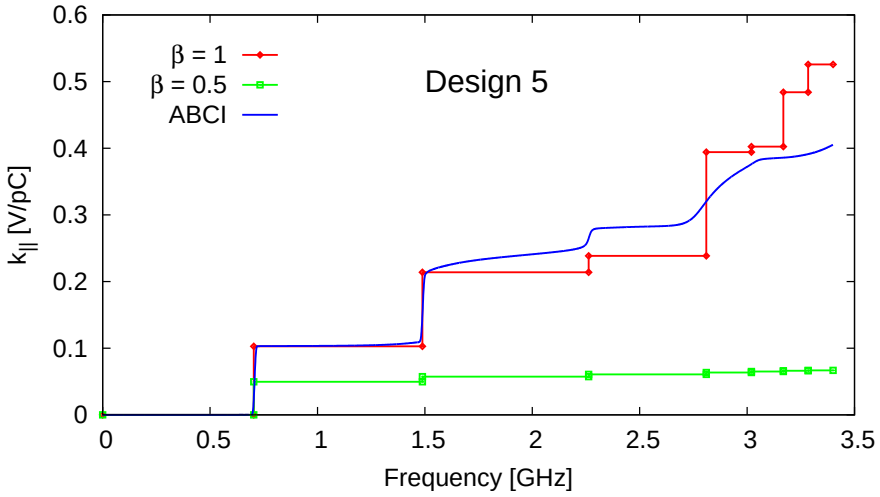

Figure E.1: Longitudinal loss factors computed for the first nine monopole modes in the gun using Eq. E.1 for both $\beta = 1$ and $\beta = 0.5$. The analytical calculation is also compared to the numerical calculation using ABCI.

modulation of the pulse train which can be expressed as

$$I(t) = \sum_{n=-\infty}^{\infty} a_n \, p(t - nT_0 - \epsilon_n) \tag{E.2}$$

where T_0 is the average separation between the pulses. We will also assume that the random variables a_n and ϵ_n are uncorrelated and follow some arbitrary distribution function.

It is of interest to calculate the spectral power density (SPD) to determine the characteristics of the modulated pulse train in the frequency domain. The SPD along with the impedance spectrum of the cavity can be used to estimate the HOM losses induced as a result of the modulation. The SPD can be

Table E.1: Frequencies and R/Q values (accelerator definition) for the first few monopole and dipole modes in the SRF gun.

Monopole Modes		Dipole Modes	
Freq [GHz]	R/Q [Ω]	Freq [GHz]	R/Q [Ω]
0.703	96.5	1.01	53.8
1.49	55.8	1.71	10.7
2.25	8.4	1.88	11.7
2.34	48.7	2.05	2.1
2.56	10.3	2.44	0.4
2.80	13.0	2.64	6.3
2.99	33.1	3.06	0.05
3.13	2.2	3.08	3.5
3.36	19.2	3.43	2.2

determined from amplitude of the Fourier transform given by

$$\mathcal{P}(\omega) = \lim_{T\to\infty} \frac{1}{2T} \langle \, | \int_{-T}^{T} I(t)\, e^{i\omega t} dt|^2 \, \rangle \tag{E.3}$$

$$= \lim_{N\to\infty} \frac{|\hat{p}(\omega)|^2}{2T_0 N} \langle \, | \sum_{n=-N}^{n=N} a_n \, e^{i\omega(nT_0+\epsilon_n)}|^2 \, \rangle \tag{E.4}$$

$$= \lim_{N\to\infty} \frac{|\hat{p}(\omega)|^2}{2T_0 N} \times \sum_{n,m} \langle a_n a_m \, e^{i\omega[(n-m)T_0+(\epsilon_n-\epsilon_m)]} \, \rangle \tag{E.5}$$

where $\hat{p}(\omega)$ is the Fourier transform of the pulse shape. Since, a_n and ϵ_n are uncorrelated

$$\langle a_n a_m \, e^{i\omega(\epsilon_n-\epsilon_m)} \rangle = \langle a_n \, a_m \rangle \langle e^{i\omega(\epsilon_n-\epsilon_m)} \, \rangle \tag{E.6}$$

For general uncorrelated amplitude modulation and time jitter, the char-

acteristic functions can be evaluated as

$$\begin{aligned} \langle a_n\ a_m \rangle &= a_0^2\ +\ \delta_{n,m}\sigma_a^2 && \text{(E.7)} \\ \langle\ e^{i\omega(\epsilon_n-\epsilon_m)}\ \rangle &= \delta_{n,m} + (1-\delta_{n,m}) \\ &\quad \times\ |\int_{-T_0/2}^{T_0/2} d\epsilon f(\epsilon) e^{i\omega\epsilon}|^2 && \text{(E.8)} \\ &= |\hat{f}(\omega)|^2 + \delta_{n,m}(1-|\hat{f}(\omega)|^2) && \text{(E.9)} \end{aligned}$$

where $\hat{f}(\omega)$ is the integral in Eq. E.8.

Using change of variables ($k = n - m$), we can rewrite

$$\begin{aligned} \sum_{n=-N}^{n=N}\sum_{m=-N}^{m=N} F(n-m) &= \sum_{k=-2N}^{k=2N} F(k) && \text{(E.10)} \\ &\quad \times\ (2N+1-|k|) && \text{(E.11)} \end{aligned}$$

Therefore, using Eqs. E.5, E.7, and E.9, we can express the SPD in the new variable as

$$\begin{aligned} \mathcal{P}(\omega) &= \lim_{N\to\infty} \frac{a_0^2|\hat{p}(\omega)|^2}{2T_0N} \left|\hat{f}(\omega)\frac{\sin\left[(N+1/2)\omega T_0\right]}{\sin\left(\omega T_0/2\right)}\right|^2 \\ &\quad +\ \frac{|\hat{p}(\omega)|^2}{T_0}\left[a_0^2(1-|\hat{f}(\omega)|^2)+\sigma_a^2\right] && \text{(E.12)} \end{aligned}$$

Taking the limit, we find that

$$\begin{aligned} \mathcal{P}(\omega) &= \frac{2\pi a_0^2|\hat{p}(\omega)|^2}{T_0^2}|\hat{f}(\omega)|^2 \sum_{k=-\infty}^{\infty}\delta\left(\omega-\frac{2\pi k}{T_0}\right) \\ &\quad +\ \frac{|\hat{p}(\omega)|^2}{T_0}\left[a_0^2\left(1-|\hat{f}(\omega)|^2\right)+\sigma_a^2\right] && \text{(E.13)} \end{aligned}$$

If the probability distribution $f(\epsilon)$ for the timing jitter is uniform or Gaussian, the characteristic function can be easily evaluated and is given by

$$|\hat{f}(\omega)|^2 = \begin{cases} \left[\frac{\sqrt{3}\sin(\omega\sigma_\epsilon)}{(\sqrt{3}\omega\sigma_\epsilon)}\right]^2, & \text{Uniform} \\ e^{-(\omega\sigma_\epsilon)^2}, & \text{Gaussian.} \end{cases} \qquad \text{(E.14)}$$

where σ_ϵ is the rms of ϵ.

E.3 Voltage Estimates for Parasitic Modes

Let the longitudinal wake potential for the parasitic mode be $W(t)$ with $W = 0$ for $t < 0$. Any dependence on the beam's transverse coordinates are assumed to be included. Model the beam as a sequence of pulses with normalized shape $p(t)$, arrival times $nT_0 + \epsilon_n$ and charges $(1 + a_n)q$. The voltage on the beam due to this mode is then

$$\begin{aligned} V(t) &= -q \sum_{n=-\infty}^{\infty} (1 + a_n)\hat{W}(t - nT_0 - \epsilon_n), && \text{(E.15)} \\ &\approx -q \sum_{n=-\infty}^{\infty} (1 + a_n)\hat{W}(t - nT_0) \\ &\quad -\epsilon_n(1 + a_n)\frac{d\hat{W}}{dt}(t - nT_0), && \text{(E.16)} \end{aligned}$$

where it has been assumed that the arrival time variation is short compared to the time scale (oscillation period) of the wake field and we have defined

$$\hat{W}(t) = \int d\tau W(t - \tau)p(\tau)d\tau, \tag{E.17}$$

as the smoothed wake potential for a single bunch.

Assume the simplest statistical model with $\langle \epsilon_n \rangle = \langle a_n \rangle = 0$, $\langle a_n a_m \rangle = \sigma_a^2 \delta_{m,n}$, $\langle \epsilon_n \epsilon_m \rangle = \sigma_\epsilon^2 \delta_{m,n}$, and $\langle \epsilon_n a_m \rangle = 0$. Also, assume a resonant wake field with a large quality factor Q_r, resonant frequency ω_r with $\omega_r \sigma_\tau \ll 1$, and shunt impedance R_r. Then the expectation value of the voltage is

$$\begin{aligned} \langle V(t) \rangle &= -\sum_{n=-\infty}^{\infty} q\hat{W}(t - nT_0), \\ &= -\sum_{k=-\infty}^{\infty} (q/T_0)Z(\omega_k)\tilde{p}(\omega_k)e^{-i\omega_k t}, && \text{(E.18)} \\ &= -\sum_{k=-\infty}^{\infty} \frac{q}{T_0} \frac{R_r}{1 - iQ_r\left(\frac{\omega_k}{\omega_r} - \frac{\omega_r}{\omega_k}\right)} \\ &\quad \times \tilde{p}(\omega_k)e^{-i\omega_k t/T_0}, && \text{(E.19)} \end{aligned}$$

where $\omega_k = 2\pi k/T_0$,

$$\hat{p}(\omega) = \int_{-\infty}^{\infty} p(t)e^{i\omega t}dt$$

is the Fourier transform of the pulse shape and $Z(\omega)$ is the impedance of the mode. The average voltage modifies the RF bucket and is a type of static beam loading.

Now consider the variance of this parasitic voltage,

$$\begin{aligned}\langle (V(t) - \langle V(t)\rangle)^2\rangle &\approx q^2 \sum_n \sigma_a^2 \hat{W}^2(t - nT_0) \\ &\quad + \sigma_\epsilon^2 \left\{ \frac{d\hat{W}}{dt}(t - nT_0) \right\}^2 \qquad \text{(E.20)} \\ &\approx q^2 \left(\sigma_a^2 + \omega_r^2 \sigma_\epsilon^2\right) \left(\frac{R_r \omega_r}{Q_r} \right)^2 \\ &\quad \times \frac{Q_r}{2\omega_r T_0} |\tilde{p}(\omega_r)|^2 \qquad \text{(E.21)}\end{aligned}$$

where we have ignored terms proportional to $\sigma_a^2 \sigma_\epsilon^2$ and assumed that the bandwidth of the parasitic resonance is narrow compared to the bunching frequency. For a Gaussian pulse of rms duration σ_t one finds $\tilde{p}(\omega) = \exp(-\omega^2 \sigma_t^2/2)$ so Eq. E.21 predicts that high frequency parasitic modes are suppressed. It is worthwhile to note that the dependence on the bunching frequency in equation (E.21) is fairly weak. For $T_0 \omega_r \gg 1$ the variance of the parasitic voltage is unaffected by a detuning of order $1/T_0$.